Ultraviolet Spectroscopy of Asteroid (4) Vesta

Jian-Yang Li[a,*], Dennis Bodewits[a], Lori M. Feaga[a], Wayne Landsman[b], Michael F. A'Hearn[a],

Max J. Mutchler[c], Christopher T. Russell[d], Lucy A. McFadden[e], Carol A. Raymond[f]

[a] Department of Astronomy, University of Maryland, College Park, MD 20742, United States

[b] Adnet Systems, NASA Goddard Space Flight Center, Greenbelt, MD 20771, United States

[c] Space Telescope Science Institute, Baltimore, MD 21218, United States

[d] IGPP & ESS, University of California at Los Angeles, CA 90095, United States

[e] NASA Goddard Space Flight Center, Greenbelt, MD 20771, United States

[f] Jet Propulsion Laboratory, California Institute of Technology, Pasadena, CA 91109, United States

New manuscript

Manuscript pages: 44

Number of tables: 1

Number of figures: 5

Submitted on: June 17, 2011

Proposed Running Head:

UV spectroscopy of Vesta

Editorial correspondence to:

Jian-Yang Li

Department of Astronomy

University of Maryland

College Park, MD 20742-2421

USA

Tel: 301-405-2103

Fax: 301-405-3538

Email: jyli@astro.umd.edu

Abstract

We report a comprehensive review of the UV-visible spectrum and rotational lightcurve of Vesta combining new observations by Hubble Space Telescope and Swift with archival International Ultraviolet Explorer observations. The geometric albedos of Vesta from 220 nm to 953 nm are derived by carefully comparing these observations from various instruments at different times and observing geometries. Vesta has a rotationally averaged geometric albedo of 0.09 at 250 nm, 0.14 at 300 nm, 0.26 at 373 nm, 0.38 at 673 nm, and 0.30 at 950 nm. The linear spectral slope in the ultraviolet displays a sharp minimum near sub-Earth longitude of $20°$, and maximum in the eastern hemisphere. This is completely consistent with the distribution of the spectral slope in the visible wavelength. The uncertainty of the measurement in the ultraviolet is ~20%, and in the visible wavelengths better than 10%. The amplitude of Vesta's rotational lightcurves is ~10% throughout the range of wavelengths we observed, but is smaller at 950 nm (~6%) near the 1-μm mafic band center. Contrary to earlier reports, we found no evidence for any difference between the phasing of the ultraviolet and visible/near-infrared lightcurves with respect to sub-Earth longitude. Vesta's average spectrum between 220 and 950 nm can well be described by measured reflectance spectra of fine particle howardite-like materials of basaltic achondrite meteorites. Combining this with the in-phase behavior of the ultraviolet, visible, and near-infrared lightcurves, and the spectral slopes with respect to the rotational phase, we conclude that there is no global ultraviolet/visible reversal on Vesta. Consequently, this implies lack of global space weathering on Vesta.

Keywords: Asteroid Vesta; Spectrophotometry; Spectroscopy; Ultraviolet observations; Hubble Space Telescope observations

1. Introduction

Asteroids are generally considered building blocks and debris left over from the formation of planetary systems. Knowledge of the composition and mineralogy of asteroids is mostly collected through spectroscopic observations and comparison with similar reflectance spectroscopic studies of meteorites under laboratory conditions. Most spectral reflectance studies have focused on optical and near-infrared (NIR) wavelengths, yet recent laboratory measurements, space missions, and remote observations with Hubble Space Telescope (HST) demonstrate that asteroidal ultraviolet (UV) spectra contain a wealth of diagnostics information that is yet to be fully understood. The existence of a UV absorption band in the spectrum of Ceres (Li et al., 2009), and the absence of one in the spectrum of Steins (A'Hearn et al., 2010; Keller et al., 2010), are indicative of substantial spectral differences among different asteroids, and/or different taxonomic classes, at these wavelengths. Recent laboratory measurements of the UV spectra of terrestrial minerals, meteorite samples, and frosts of volatiles have shown many potentially diagnostic absorption features in the UV region (see e.g. Cloutis et al. 2008; Hendrix & Vilas 2006). Space weathering is believed to lower the albedo in the visible, subdues the absorption features in the visible and NIR wavelengths, and flattens out the UV region resulting in brightening and bluing in the UV relative to fresh materials (e.g., Chapman, 2004; Hendrix and Vilas, 2006).

The International Ultraviolet Explorer (IUE) telescope collected the first set of UV reflectance spectra of about 50 asteroids about three decades ago (Butterworth et al., 1980; Butterworth and Meadows, 1985). In addition to these IUE observations, only a few scattered observations of some asteroids in the UV exist. (2867) Steins and (21) Lutetia were observed

with HST and with the ALICE instrument during Rosetta spacecraft's flybys (A'Hearn et al., 2010; Weaver et al., 2010; Stern et al., 2011). Additionally, HST acquired the UV spectrum of (1) Ceres (Parker et al., 2002; Li et al., 2006; 2009), and (596) Scheila was observed with the Swift Gamma-ray Burst Observatory (Bodewits et al., 2011a). In the mean time, laboratory measurements of the UV reflectance spectra of meteorites and candidate asteroid composition minerals have gradually been collected (e.g., Wagner et al., 1987; Cloutis et al., 2008). Despite all the development in laboratory work and UV observations of asteroids, our understanding of asteroid reflectance spectra in this wavelength region is still in an early stage.

As the second largest asteroid by mass, asteroid (4) Vesta has drawn the attention of planetary scientists for a long time. It was identified as the most probable source of a class of meteorites, the abundant howardite-eucrite-diogenites (HEDs) collection (McCord et al., 1970). Vesta is recognized as the largest differentiated asteroid in the solar system that has a basaltic surface, having undergone a thermal evolution similar to terrestrial planets in its early history (e.g., Keil, 2002; Pieters et al., 2005). Its unique position in the asteroid population secured its scientific significance to understanding the formation and evolution of terrestrial planets. This is the fundamental motivation of NASA's Dawn mission, which is currently at Vesta for a year long rendezvous. In orbit around it, Dawn will perform a detailed survey of its surface characteristics, internal structure, and elemental abundance targeted to understanding its formation and evolution (Russell et al., 2007)

Rotationally resolved IUE spectra of Vesta from IUE showed single-peaked rotational lightcurves in the UV from 240 nm to 320 nm, indicating brightness changes dominated by surface compositional variations rather than shape in lightcurves (Festou et al., 1991; Hendrix et

al., 2003). The UV albedo of Vesta is less than 0.10, much lower than its visible albedo of ~0.37 (Schevchenko and Tedesco, 2006). While the close analogy between Vesta and HED meteorites at optical and NIR wavelengths has been interpreted as indicating relatively minor, global-scale space weathering (e.g., Keil, 2002; Pieters et al., 2005), Hendrix et al. (2003) proposed that the UV spectra and lightcurve reversal of Vesta do indicate significant space weathering.

Vesta has not been studied in the UV since the early IUE observations, now over 30 years ago. With the arrival of Dawn at Vesta in July 2011, better knowledge of this asteroid in the UV becomes necessary both to help Dawn plan its observations in the UV and to provide context for the interpretation of the soon-available Dawn data. The study of Vesta in the UV will expand the detailed investigation of Vesta's mineralogical characteristics and history, including the puzzling space weathering for this particular case of Vesta, to the UV region for asteroid science in general.

We hereby report our recent observations of Vesta with HST Wide Field Camera 3 (WFC3) and the UV-Optical Telescope (UVOT) onboard Swift. We will describe our observations and data reduction and measurements in the next section (Section 2), then discuss the spectrophotometry of Vesta in the UV into visible wavelengths by combining the HST/WFC3, Swift/UVOT, and IUE observations in Section 3. Section 4 includes a simple mixing model invoked to explain the observed UV-visible spectrum of Vesta, and a discussion about space weathering on Vesta based on our observations. The conclusions are summarized in Section 5.

2. Observations and data reduction

2.1 Hubble Space Telescope

2.1.1 Photometry

HST observed Vesta in February 2010 with the WFC3 through seven filters centered from 225 nm to 953 nm, as summarized in Table 1. The exposures through filters F373N, F469N, F673N, and F953N cover one full rotation of Vesta, while the images through F225W, F275W, and F336W only cover one rotational phase at sub-Earth longitude of ~250°. In our calculations of the Vesta longitude/latitude, we adopted the pole orientation of Vesta revised by Li et al. (2011), which represents a change of about 4° from those previously reported by Thomas et al. (1997) and Drummond and Christou (2008). This minor change in the pole orientation would only cause up to a few degrees shift in the sub-Earth and sub-solar coordinates on Vesta, and therefore does not affect the comparisons of our work with all previous works based on the pole determined by Thomas et al..

Starting from the pipeline-calibrated images delivered by HST, we measured the total flux from Vesta from all images within a circular aperture of 40 pixels (1.6") in diameter. The sky background was typically a few counts, negligible compared to more than 1000 counts on the disk of Vesta. The correction for aperture size due to the point-spread-function (PSF) for the extended disk of Vesta (0.54" in diameter for our observation) is different from that for a point source. We extracted the aperture photometry of Vesta with a series of diameters from 0.8" to 8.0", as well as for the model PSF generated by TinyTIM (Krist and Hook, 2004). Assuming an 8.0" aperture (much larger than the angular size of Vesta for our observation) captures more than 99% of the flux, we normalized the energy enclosure curve of Vesta with that of the PSF at 8.0"

aperture, and derived the PSF correction for 1.6" aperture photometry of Vesta. The correction factors range from 1.081 through F225W filter to 1.063 through F953N filter (Table 1). The red leak for WFC3 in the F225W filter is less than 0.3% for a solar type star for flux longward of 400 nm (Rajan et al., 2010). We estimated the red leak of F225W for Vesta by modulating a solar spectrum E490 (E-490-00, American Society for Testing and Materials Airmass 0 reference spectrum, DOI: 10.1520/E0490-00AR06) with a preliminary reflectance spectrum of Vesta that we constructed using our photometric measurements in the visible wavelengths, the SMASS II spectrum, and IUE spectrum, and folded it through the filter transmission curves. The fraction of the flux longward of 400 nm is estimated to be ~2.8% for Vesta, comparable to that of a star with an effective temperature of 4000 K. We corrected for the red leak in the F225W photometry by subtracting 2.8% flux from the total measured flux. The red leak for F275W and F336W filters at this effective temperature is negligible, amounting only to 0.3% and 0.01%, respectively.

2.1.2   Albedo

The geometric albedo of Vesta, p, is calculated as,

$$p = \frac{F_V \, r_\odot^2 \, \Delta^2}{F_\odot \, R^2 f(\alpha)}$$

where F_V is the measured flux of Vesta; $F_\odot$ is solar flux through the same filter at 1 AU; $r_\odot$ and Δ are the heliocentric distance and Earth range of Vesta at the time of observation, R is the equivalent radius of Vesta, and $f(\alpha)$ is the phase function of Vesta. We took the high-resolution solar spectrum E490 and the synthetic filter transmission curves provided by HST (Dressel, 2010) to calculate the equivalent solar flux density through each filter we used:

$$F_\odot = \frac{\int S(\lambda)\, T(\lambda)\, \lambda\, d\lambda}{\int T(\lambda)\, \lambda\, d\lambda}$$

where $S(\lambda)$ is solar spectrum; and $T(\lambda)$ is the composite filter transmission curve including CCD quantum efficiency and telescope optics. The values of $F_\odot$ for all seven filters we calculated are listed in Table 1.

A phase function correction is critical to deriving the geometric albedo, but different phase functions may be used. For example, Festou et al. (1991) used a phase function of a constant slope of 0.036/deg for the IUE observation at 17° phase angle, while Roettger and Buratti (1994) used a Hapke phase function of average S-type asteroids (Helfenstein and Veverka, 1989) for the same data. We assume the same phase function across the whole range of wavelengths of our observations, and fitted the ground-based photometry data of Vesta in the V-band included in the Asteroid Photometry Catalog dataset (Lagerkvist et al., 1995) archived in the Planetary Data System Small Bodies Node with the IAU HG phase function model (Bowell et al., 1989), and found a G parameter of 0.28. Phase reddening is expected to cause steeper phase slope at shorter wavelengths (Reddy et al., 2011). However, phase reddening is poorly understood and the lack of data prevents us from correcting for this effect in our data. We will return to this issue in Section 2.4 in the comparison between observations from different instruments. The cross-sectional area of Vesta at the sub-Earth latitude of our observation (~20°) was calculated using the shape model as well as the pole orientation (Li et al., 2011) to have an equivalent radius of 259 km. With only ~3% difference between the long-axis and the intermediate axis, we ignored the change in the long-axis in the projected disk of Vesta, and used a constant cross-sectional area in our calculation.

Since the solar flux drops by two orders of magnitude between 400 nm and 200 nm, the broadband geometric albedo measured in this range depends significantly on the transmission profile of the filter and the illumination source used. The measured albedo is weighted more towards longer wavelengths where solar flux is stronger. In order to best compare the broadband albedo with spectroscopic measurements, we invoke the "equivalent wavelength" of the broadband albedo, defined as the transmitted source flux weighted average wavelength of the filter transmission:

$$\lambda_E = \frac{\int S(\lambda)\, T(\lambda)\, \lambda\, d\lambda}{\int T(\lambda)\, d\lambda}$$

where $S(\lambda)$ is the solar spectrum, and $T(\lambda)$ is the filter transmission curve. Since the red leak of WFC3 broadband filters in the UV is only up to 3% for F225W and negligible for longer wavelength, its effect on the equivalent wavelength is ignored. The equivalent wavelengths of all the filters we used are listed in Table 1. For narrow band filters, the equivalent wavelengths are almost independent of source spectrum.

2.2 Swift

2.2.1 Broadband photometry

Swift observed Vesta on April 5 and 20, 2011 UT (Table 1). Our observations uses the UV-Optical Telescope (UVOT) that provides a 17 × 17 arcminute field of view with a plate scale of 1 arcsec/pixel. The PSF of UVOT has a FWHM of 2.5" (Poole et al., 2008). We used the UVW2 and UVM2 filters, and the UV grism to acquire low-resolution ($\lambda/\delta\lambda = 100$) spectroscopy between 200 and 330 nm. The grism was operated in 'clocked mode' to suppress background stars and the dispersion axis was oriented at a position angle of ~260°. The asteroid was not

tracked, and the proper motion is ~10" over our ~700 s grism exposures, ~2" for UVM2 exposures, and ~0.3" for UVW2 exposures, with varying effects on the photometry, which will be discussed later.

We measured the broadband photometry through UVM2 and UVW2 from the standard 5" radius aperture (Poole et al., 2008). Compared to the size of PSF, the smearing in images is small and barely visible in UVM2 images, and the effect on photometry is negligible. The brightness of Vesta results in significant coincidence loss (Poole et al., 2008), which we estimated to be 0.7 mag at UVW2 and 0.06 mag at UVM2 and corrected for in our photometric measurements. While UVM2 only suffers a minimal amount of red leak for solar spectrum, UVW2 has a significant red leak. We took the filter transmission profile (Breeveld et al., 2011), and multiplied it with both solar spectrum (E490) and the solar spectrum reddened by a trial Vesta spectrum in the UV-visible wavelength (based on our HST measurements and IUE observations) to estimate the fraction of flux coming from long wavelength. For UVM2, about 0.6% flux comes from wavelength longer than 400 nm for a solar spectrum, and 2.6% for a Vesta-reddened solar spectrum; for UVW2, it is about 25% for a solar spectrum, and 50% for a Vesta-reddened spectrum. Based on those factors, we removed the out-of-band flux from the total Vesta's flux measured from imaging photometry, and then only used the in-band solar flux to derive the geometric albedo for the two filters we used. Red leak also affects the effective wavelength. Following the same procedure described in the previous section, and using the solar spectrum E490, we calculated the expected solar flux through the UVOT filters, as well as the effective wavelengths listed in Table 1. With the effort to remove red leak from the filters using the fraction of flux below 400 nm, it is reasonable to set the flux to zero beyond 400 nm in calculating the effective wavelengths.

The photometric results are subject to several possible systematic uncertainties. The absolute calibration of both UVW2 and UVM2 is accurate to within 0.03 magnitudes. Shot noise and background subtraction uncertainty, as well as the aperture and coincidence loss correction errors, are all included in the listed uncertainties. For the red leak, we estimated the uncertainty of 10% after correction. All sources of errors are combined in a quadrature manner.

2.2.2 Grism spectroscopy

We extracted the asteroid's spectrum from a rectangular region 13 pixels wide, centered on the asteroid's position. Swift did not track the asteroid, and the combined smearing due to the orbital parallax and apparent motion of Vesta is ~20 pixel along the dispersion axis, and ~7 pixels in the perpendicular direction. The PSF along the spatial direction is about ~8 pixels in FWHM, and we found that the smearing affects the photometry at a 4% level. The smearing along the dispersion axis effectively degrades the spectral resolution to ~5 nm. We accounted for this in the removal of solar spectrum by binning Vesta's spectrum in 10 nm intervals, and by smoothing the solar spectrum with a 10 nm boxcar average. The brightness of the asteroid resulted in saturation or significant coincident loss of the spectrum beyond 290 nm. Two of the four spectra we acquired are contaminated by background stars in the dispersion tracks. We were able to subtract the stellar spectrum from Vesta's spectra obtained by comparison with a grism image where the background star did not fall onto Vesta's dispersion track. The subtraction resulted in a spectrum of Vesta that is in good agreement with the uncontaminated spectra (Fig. 1). The uncertainty of the absolute radiometric scale of Vesta's spectrum is 25% (Bodewits et al., 2011b). The relative pixel-to-pixel noise in the spectrum is typically less than 2% after binning.

The reflectance spectrum and geometric albedos were derived using the methods and solar spectrum discussed in Section 2.1.2. The sub-Earth longitude of Vesta during Swift observation is similar to that during HST observations except that it is on the opposite hemisphere. Therefore the same equivalent radius of Vesta as used for the HST data is used here. The geometric albedo spectra of Vesta measured by Swift are shown in Fig. 1.

2.3 International Ultraviolet Explorer

IUE observed Vesta in 1990 and earlier. In order to compare the IUE spectra to our new observations, we re-processed the IUE spectra using the same procedure, the same solar spectrum, and the same phase function in the derivation of geometric albedos as were used for the HST and Swift data.

The flux spectra of Vesta were extracted from all relevant IUE data (NEWSIPS) that are available through the Multimission Archive at STScI (MAST) website. We applied the corrections to all Vesta's spectra to derive absolute flux following Massa and Fitzpatrick (2000) to all Vesta spectra. This correction is in general at a 5% level. The same set of spectra as used by Hendrix et al. (2003) were used in our analysis. Earlier IUE data are either of poor quality or incomplete, and are not used in our study. The geometric albedo is derived following the same procedure described earlier with the same phase function and the solar spectrum E490. The sub-Earth latitude of Vesta during IUE observation was about 10° North. The difference in the cross-sectional area of Vesta from HST and Swift observation is at a 1% level, and is therefore ignored.

2.4 Comparisons between three instruments

Fig. 2 shows the geometric albedo measured from all three instruments at various wavelengths, combined with SMASS II data (Bus and Binzel, 2003) scaled to match our HST photometry at 469 nm and 673 nm. The visible geometric albedo of Vesta was reported to be 0.42±0.05 at visible wavelength as measured from IRAS (Tedesco et al., 2002), assuming an equivalent diameter of 468 km. Corrected to the size measured from HST (260 km, Thomas et al., 1997), the IRAS measurement is equivalent to a geometric albedo of 0.34, consistent with our HST measurement (Fig. 2a). Shevchenko and Tedesco (2006) reported a visible geometric albedo of 0.37 for Vesta based on an occultation-determined size that is consistent with HST observations. This value is also consistent with our measurements and the adjusted IRAS measurements.

Our UV measurements using WFC3 yield geometric albedos of Vesta of 0.12 at 253 nm, 0.15 at 282 nm, and 0.21 at 338 nm. This is almost twice the albedos of 0.065 at 245 nm and 0.075 at 270 nm as previously reported by Festou et al. (1991) and Roettger and Buratti (1994). These differences can be partially explained by the different phase function corrections we used and possibly the equivalent size of Vesta used. Applying the phase function we used for the Swift and HST data, we found geometric albedos of 0.074 at 245 nm and 0.085 at 270 nm. We assumed here that an equivalent radius similar to ours was used, as this parameter was not reported in their paper. Hendrix et al. (2003) reported the reflectance of Vesta at $17°$ phase angle to be between 0.04 and 0.07 within 240 nm and 320 nm using an equivalent radius similar to ours. Applying our phase function, this translates to a range of 0.08 and 0.14 geometric albedo, in much better agreement with our measurements, yet still lower by about 25% (Fig. 2b).

Roettger and Buratti (1994) reported geometric albedos similar to those reported by Festou et al., but used a different phase function. Correcting with the phase function and equivalent radius of Vesta (234 km) that we used resulted in even smaller albedos, deviating further from those we derived.

Another factor that affects the comparisons between observations made under different geometries is phase reddening. Vesta shows a redder reflectance spectrum in the visible wavelengths when observed at higher phase angles than at lower phase angles (Reddy et al., 2011). A consequence of this effect is a steeper phase function at shorter wavelengths than at longer wavelengths. Our HST data were obtained at ~5° phase angle, the IUE data were obtained at ~17° phase angle, and the Swift data was obtained at ~26° phase angle. We used the same phase function derived from V-band photometric data to apply phase correction to all the data across the whole spectral range from 220 nm to 950 nm to zero phase angle. Therefore, the phase correction we applied in the UV might underestimate the slope of the phase function in the UV. This contributes to the discrepancy between the measurements of UV albedos from three different phase angles, and is consistent with the fact that the albedos measured at the highest phase angle from Swift have the lowest values, and those measured at the lowest phase angles from HST have the highest values. A quantitative estimate based on the formulae proposed by Reddy et al. (2011) shows that at least 8% difference between Swift and HST observations, and at least 3% difference between IUE and HST observations can be accounted for by phase reddening, assuming those formulae are valid in the whole range of wavelengths and range of phase angles of our study including inside the opposition surge (phase angle < a few degrees).

To rule out that the discrepancy between the archival and new observations were due to other assumptions made while deriving the geometric albedo, we took one IUE flux spectrum (LWP18950) that is close to the median of the rotational lightcurve, and passed it through WFC3 F225W and F275W filter to calculate the corresponding broadband fluxes based on IUE spectrum. The predicted WFC3 flux from IUE spectrum should be good to 25% level. After correcting for the observing geometry and phase angle (no phase reddening considered), the total WFC3 broadband fluxes calculated from IUE spectrum are lower than WFC3 measurement by 20%. This agrees with what we found in comparing the geometric albedo derived from WFC3 and IUE observations assuming the same phase function correction and equivalent size of Vesta (Fig. 2b).

Could the differences in Vesta's UV flux measured using different instruments be due to the variation in the input solar flux? The IUE observation was made near a solar maximum in 1990, while the Swift and HST observations were both obtained near a solar minimum. While the solar flux does vary more in the UV than in longer wavelengths with solar cycles, the variation is about 10% at 200 nm, 5% at 250 nm, and less than 1% at wavelengths longer than 300 nm (Lean, 1989). While there is no solar spectral data available for the time of IUE observations, the variations in solar flux from solar maximum to solar minimum suggests that the albedo spectra of Vesta derived from IUE data overestimate the albedo of Vesta by ~10% at 200 nm, and by ~1% at 300 nm. This is consistent with the measurement that Vesta's UV albedos from Swift is 10%-20% lower than those from IUE, and also explains the slight differences in the spectral slopes measured at different epochs (phase reddening being another possible factor, but hard to quantify).

Combining all the possible sources discussed above that may cause this discrepancy, we concluded that the geometric albedo measurements in the UV from three instruments at three epochs and observing geometries are consistent with each other. The difference is caused by the combination of phase reddening, solar spectrum, and instrumental difference. Considering the uncertainties of the absolute flux calibration of the Swift grism of ~25% (Bodewits et al., 2011b), IUE spectrum 15-20% (Nichols and Linsky, 1996; Massa and Fitzpatrick, 2000), and that HST UV measurements were made through broadband filtering configuration, the three instruments actually confirm each other's derived Vesta UV albedos. Given the fact that HST observations were performed at the lowest phase angle of ~5°, and that the absolute flux calibration of broadband photometry should be better than that for spectroscopic observations, we consider that the UV geometric albedos derived from HST observations are the most reliable.

3. Results

3.1 UV-visible reflectance of Vesta

The UV albedo of Vesta of about 0.08 at 250 nm is comparable to other asteroids. The albedos of asteroids in the UV wavelengths are generally low. IUE measured the UV spectra of 45 asteroids of almost all major asteroid types including C, S, V, M, etc. (Butterworth and Meadows, 1985; Roettger and Buratti, 1994). Only (44) Nysa (E-type) has a geometric albedo of ~0.28 at 250 nm; all others of various types have geometric albedos below 0.12, and mostly between 0.03-0.08. The most recent measurement of Ceres (G-type) yielded a geometric albedo of ~0.03 near 280 nm (Li et al., 2006; Rivkin et al., 2011), which is consistent with values previously reported from IUE (Butterworth et al., 1980; Butterworth and Meadows, 1985; Roettger and Buratti, 1995). Asteroid Steins (E-type) has a relatively high geometric albedo of

~0.15 at 250 nm (Keller et al., 2010; A'Hearn et al., 2010). Lutetia, which is specified as an M-type in Tholen's taxonomy but an X-type by Bus and Binzel (2002) for its unusual spectrum and albedo in the visible, has a geometric albedo of ~0.1 at 250 nm (Weaver et al., 2010; Stern et al., 2011). Asteroid (596) Scheila, which showed an ejecta plume in December 2010 that is mostly consistent with an impact, is a T-type asteroid (Bus and Binzel, 2002) and has an albedo of 0.02-0.03 between 200 nm and 300 nm (Bodewits et al., 2011a). It appears that there is little correlation between the UV albedo of these asteroids and their taxonomic types. Whether this suggests that UV albedos are uncorrelated to taxonomy types, or there are presently insufficient data in the UV to draw a conclusion, is an important question to answer with future systematic surveys of asteroids and laboratory measurements in the UV.

Although almost all of the asteroids with UV observations have had their geometric albedos and spectra observed in the visible as well, only those mentioned above have either been studied in parallel with both UV and visible spectroscopy or have had their UV and visible spectra systematically discussed in a compilation. While in the visible all of them have mostly linear and featureless reflectance spectra with a weak red slope, the characteristics of their spectra from visible into UV wavelengths are completely different. Vesta has a strong absorption band near 1-μm starting near 750 nm diagnostic of mafic minerals, a linear red slope of about 7-10%/100 nm in the visible outside of the 1-μm band, and then a very steep and almost linear spectrum into UV until 220 nm (Fig. 2). By comparison, Ceres has a flat spectrum through the visible and a steep drop starting from just longer than 400 nm wavelength, leading to a deep (~60%) absorption band centered at 280 nm (Li et al., 2006; 2009). Steins has a weak red slope of about 7%/100 nm in the visible, and then a gradual drop in albedo from 0.3 at 500 nm to 0.05 at 200 nm, by almost 85% (A'Hearn et al., 2010). Lutetia also has a ~2%/100 nm red slope

in the visible wavelengths, and a drop of 30% from 0.15 at 350 nm to 0.1 at 300 nm then stay almost flat into 150 nm (Weaver et al., 2010; Stern et al., 2011). Scheila is very red in the visible with almost a 40%/100 nm slope, and might have an absorption band of about 15% centered at 350 nm (Bodewits et al., 2011a). Given the different spectral shapes of these asteroids from visible to the UV wavelength, it is valuable to combine the visible spectroscopy with the UV wavelength, and systematically study the spectral characteristics of a large sample of asteroids to ultimately expand the spectral range of the current taxonomy scheme to include the UV region.

3.2 Rotational lightcurve

Fig. 3a shows the geometric albedo measured from HST/WFC3 and Swift images plotted with respect to sub-Earth longitude; Fig. 3b shows IUE spectra grouped into three wavelength bins and plotted with respect to longitude. The shapes of the four full lightcurves at 373, 469, 673, and 953 nm are consistent with those reported before (e.g., Blanco and Catalano, 1979). The UV lightcurves have similar shapes as well. All lightcurves are dominated by albedo rather than cross-section variations, with a darker western hemisphere and a brighter eastern hemisphere (Binzel et al., 1997; Li et al., 2010). The amplitudes of the lightcurves remain ~10% in 373 nm to 673 nm, ~6% at 953 nm near the center of the characteristic 1-μm absorption band of its basaltic surface, and ~10% in the UV. The lightcurve maxima in the four full lightcurves from WFC3 occur at almost the same longitude near 100° E. The lightcurve minimum appears to be flat between 300° E and 0° in 953 nm, and occurs near ~300° E or slightly to the west for 673 nm and shorter wavelengths into the UV. The HST snapshot geometric albedo measurements at 336 nm, 275 nm, and 225 nm correspond to sub-Earth longitude of 280° to 290°, near the lightcurve minima in other wavelengths.

Based on the IUE observations, Hendrix et al. (2003) reported the exchange of Vesta's lightcurve maximum and minimum from visible wavelength to UV, and attributed this effect to space weathering. However, the sub-Earth (west) longitudes we calculated from the reported IUE observing times are consistently greater than those listed in Table 1 in Hendrix et al. (2003) by ~133°. This shifts the lightcurve minimum to about 290° E, and the maximum to about 120° E, *consistent with the lightcurves in the visible wavelengths*. Festou et al. (1991) phased the same IUE UV spectra and simultaneous photometric data in near-*B* band obtained with the FES camera onboard IUE, and reported that the UV lightcurve and near-*B* band lightcurve are slightly out-of-phase by up to 20°. Taking the coordinate system defined by Li et al. (2011), the sub-Earth longitude at the zero rotational phase in Festou et al. is 85°, putting both the near-*B* band lightcurve and the UV lightcurve in good agreement with the lightcurves we observed from WFC3. The amplitude of the Festou et al. near-*B* lightcurve of ~11% is the same as the amplitude of our lightcurve at 469 nm. In addition, Swift photometric data (Fig. 3a), although sparse, are not consistent with a reversal of maximum and minimum between UV and visible lightcurves. The rotational period of Vesta was measured to a precision better than 0.004 seconds (Drummond et al., 1998), resulting in an uncertainty of only ~2° in longitude over 20 years. We therefore concluded that, although Vesta's lightcurves at wavelengths between 240 nm and 953 nm appear to be slightly shifted in phase, there is no evidence for a complete lightcurve reversal at those wavelengths. The geometric albedos of Vesta at 225 nm, 275 nm, and 336 nm derived from our HST observations are near the minimum of the rotational lightcurves of Vesta, and the maximum brightnesses at those wavelengths are about 10% higher.

3.3 Rotational variation of the UV-spectrum

Further exploring rotational variations of the UV spectrum of Vesta, we measured the UV spectral slope of Vesta from IUE data within 240-320 nm (Fig. 5). The UV slope appears to have a dip (relatively blue) near 10° in longitude, and is relatively high (red) in other longitudes, with the highest values concentrated in the eastern hemisphere from 80° to 160° in longitude. The most recent color ratio map in the visible wavelength shows that, from 430 nm to 670 nm, the reddest area on Vesta is concentrated from 60° to 180° in longitude; the western hemisphere from 180° to 280° is slightly redder than the average surface, and the bluest area is only concentrated in 0° to 40° (Li et al., 2010). This is entirely consistent with the UV slope we observed from 240 nm to 320 nm, indicating that the slope variation with respect to longitude is more likely real than noise. This suggests that the same spectral slope variations of Vesta with respect to longitude in the visible wavelength continue into UV wavelength, and the spectral slope map of 673 nm/439 nm (Li et al., 2010) in visible wavelengths is probably still valid in the UV.

While the visible color slope map of Vesta (Li et al., 2010) shows about 15% variation at a 39 km/pixel scale, Fig. 5 shows that at a hemispheric scale, the UV slope changes at least 30% from minimum to maximum. This is evidence that the color variation on Vesta in the UV is larger than that in the visible. IUE lightcurves also show comparable or slightly higher amplitudes than those in longer wavelengths (Fig. 3b).

4. Discussion

4.1 Spectral mixing model

Vesta's prominent spectral features in the wavelength regime studied here include a sharp absorption edge below 400 nm which is characteristic of charge transfer absorptions and a broad absorption band near 950 nm attributed to electronic absorptions in ferrous iron in pyroxene (McCord et al. 1970; Wagner et al. 1987). From the rotational variation of Vesta's 1-μm and 2-μm mafic bands, including their band centers and the band area ratio, it is generally concluded that the surface of Vesta is mostly covered by brecciated howardite with eucritic and diogenitic minerals concentrated in the western hemisphere and eastern hemisphere, respectively (Gaffey, 1997; Binzel et al., 1997). The spectral characteristics of the UV region are shaped by the combination of multiple charge transfer absorptions superimposed comprising the UV absorption edge, including Fe-O, Fe^{2+}, Ti^{4+}, Fe-Ti, and Fe^{2+}-O, etc. (Wagner et al., 1987; Cloutis et al., 2008). Opaque materials usually do not have UV absorption edge. While our data do not have the spectral resolution near the 1-μm band to permit us to fit a unique pyroxene abundance model, they cover both the UV and visible wavelengths. We examined the laboratory UV-visible spectra of various minerals and the existing mixing model for Vesta over the whole spectral range against our data, and show that it is necessary to incorporate multi-wavelength studies in order to validate any spectral fit. Optimizing spectral fits to a limited wavelength region can lead to misinterpretation of the compositional constituents.

Variations in Vesta's lightcurve are dominated by compositional variation rather than shape. In order to investigate Vesta's average surface composition, we adopted a spectrum of Vesta using the mid-points of the UV and visible lightcurves. We approached our fitting

analysis by choosing the most likely compositional candidates available in the laboratory reflectance spectral databases. Spectra were retrieved from Wagner et al. (1987) for UV wavelengths and from RELAB for visible wavelengths for howardite (Bununu and EET87503, respectively) and diogenite mineral powders (Johnstown for both). Wagner et al. acquired spectra for a single particle size for each mineral in the UV. The powders were sieved to < 150 microns. In contrast, spectra were acquired for several particle sizes at RELAB. In order to investigate the spectral effects of grain size from 300 nm through 1000 nm, we scaled the RELAB reflectances to Vesta's geometric albedo derived from the mid-point of the HST observations at 469 nm. In Fig. 4a, the small grained howardite spectrum plotted is an uniform, linear mix of fine powder wet and dry sieved to 25 microns. The large grained spectrum is for powder sieved to 250 microns. The diogenite powders are sieved to 25 and 75 microns, respectively. The finer grained material fits better in both wavelength regimes, consistent with previous studies (Hiroi et al., 1994). This is consistent with previous conclusions that the surface of Vesta is dominated by brecciated howardite and polymict eucrite (Gaffey, 1997). Both howardite with grain size > 25 μm and diogenite resulted in deeper 1-μm bands than observed, although their UV slopes match observations well. Weathered diogenite, which has a weaker band than the unweathered diogenite, could fit the 1-μm band but not the spectral color.

Because the finer grained spectra from RELAB do not extend down to 200 nm, we created a composite reflectance spectrum of howardite using the fine grained RELAB reflectances above 320 nm, again scaled to the HST geometric albedo mid-point at 469 nm, and the UV reflectance spectra published by Wagner et al. (1987) below 320 nm, scaled to the IUE geometric albedo at 320 nm, so that the fit at long and short wavelengths was optimized. The same thing was done for diogenite. By linearly mixing 20% of the composite diogenite with 80%

of the composite howardite, only slight differences are found as compared to 100% fine particle howardite (Fig. 4b). The differences are well within the error bars and absolute calibration of the instruments in the UV. The strength of the 1-μm band put a strong constraint on the relative abundance of diogenite, with more diogenite resulting in too strong an absorption to match Vesta's visible spectrum.

We re-examined the Hendrix et al.'s (2003) fit to the IUE data with a linear combination of Wagner et al.'s (1987) sample powders. The best fit for the eastern hemisphere was a linear combination of 54% howardite, 36% diogenite, and 10% fayalite. For the western hemisphere, their best fit included 90% howardite and 10% diogenite. In Fig. 4b, we plot these same linear combinations of reflectances, scaled to the HST data point at 469 nm, with the HST, Swift and IUE geometric albedos. The 1-μm absorption band is poorly fit by the larger particle mix. However, the UV region is best fit with their howardite, diogenite, fayalite mixture.

In conclusion, a single fine grained howardite (grain size <25 μm) fits our Vesta spectrum from 220 nm to 950 nm, including the spectral slope in the UV and in the visible, as well as the short wavelength side of the 1-μm band. Space weathering is not required here to match the whole UV-visible spectrum. Although the spectral uncertainty in the UV and the spectral resolution in the visible do not allow us to fit the exact fraction of possible pyroxene components or to study the rotational variations of surface composition, it is evident that the UV region provides important additional constraints on the interpretations of the reflectance spectrum of Vesta. The different characteristics of UV spectra of the asteroids that have been intensively studied recently, including Ceres, Steins, Lutetia, and Scheila, suggest the necessity

to systematically study the UV absorption features of asteroids, as well as the laboratory measurements of meteorite samples and terrestrial minerals and ices.

4.2 Space weathering

Space weathering is the time-dependent alteration of the surfaces of airless bodies when exposed in space environment, changing the optical properties of the surfaces, including darkening of albedo, reddening of spectral slope, and weakening of absorption features in the visible and NIR. It was originally invoked to explain the spectral differences between lunar soils and rocks, and between returned lunar samples and telescopic observations of the sampling sites on the Moon (e.g., Chapman et al., 2004, and references therein). The more weathered lunar soil samples display much redder spectra than do the freshly crushed lunar rock samples. Vapor deposition of nanophase iron on the surfaces of regolith grains induced by micrometeorite impact, solar wind particle bombardment and implantation is generally considered to be the primary causes of the change in the optical properties of weathered surfaces (e.g., Pieters et al., 2000). The flybys of the Galileo spacecraft with two asteroids, (951) Gaspra and (243) Ida, as well as the rendezvous of the NEAR Shoemaker spacecraft with a near Earth asteroid, (433) Eros, all being S-type asteroids, provided direct evidence of weathering on this class of asteroids (Chapman et al., 1996; Clark et al., 2001). Based on the analysis of IUE and HST observations of S-type asteroids and laboratory measurements of lunar samples in the UV, Hendrix and Vilas (2006) showed that space weathering manifests itself in the UV as bluing the spectrum as oppose to reddening in the visible-NIR. They also showed that the UV spectrum is more sensitive than visible-NIR spectrum, and therefore a better probe, to space weathering than the visible-NIR spectrum.

Vesta's basaltic surface is similar to that of the Moon, which is severely weathered. Therefore the lack of any evidence of space weathering on Vesta as suggested by the nearly perfect match between HED meteorite spectrum and Vesta's spectrum (McCord et al., 1970) is always surprising. Both observations of S-type asteroids in the inner main belt and laboratory ion irradiation experiments with meteorite samples suggested that the surface of Vesta should be significantly darkened and reddened with respect to HEDs in 10^6 yr, a relatively short time scale compared to impact resurfacing time scale (e.g., Nesvorny et al., 2005; Vernazza et al., 2006). A few explanations have been proposed to explain the apparent lack of space weathering on Vesta, including resurfacing by a recent large impact, magnetic field shielding, compositional and environmental difference between Vesta's surface and the lunar surface, etc., all with their own deficiencies or aspects that are hard to prove (e.g., see Chapman et al., 2004). On the other hand, Li et al. (2010) proposed that a few small isolated areas on Vesta might show signs of weathered/fresh surfaces based on the albedo and color ratio maps derived from HST observations.

As discussed in the previous sections, Vesta's lightcurve amplitude is almost constant in the UV-visible region outside of the 1-μm band; the phasing of its lightcurve maximum and minimum with respect to longitude remains nearly unchanged throughout the UV-visible region; and the longitudinal variation of its UV spectral slope is entirely consistent with that in the visible. What do they imply about the space weathering on Vesta?

If there is space weathering on Vesta, too little to be detected in the visible but evident in UV (Hendrix and Vilas, 2006), then its UV slope would show a slight bluing relative to its visible slope. In this case, a smaller color variation (lightcurve amplitude) is expected in the UV

than in the visible. Li et al. (2010) argued that the color heterogeneity on Vesta might be mostly compositional rather than maturity related because of the correlation between a relatively redder spectral slope and the relatively stronger 1-μm band depths in most of the surface, except for a few small areas that are either the bluest or the reddest. They also suggested that the bluest area near 20° longitude (#13 in their annotated maps) might consist of fresh, newly exposed materials; and the extremely red area (#15) might be the most weathered terrain. If this is the case, and space weathering does make UV slope bluer (Hendrix and Vilas, 2006), then we would see a relatively steep spectral slope at 20° longitude in the UV, exactly opposite of what we observe in Fig. 5. Therefore, we do not find any evidence for space weathering in the UV-visible region of our analysis. Furthermore, the inconsistency between the expected UV and visible spectral slopes and observations of area #13 and #15 either undermines the interpretations by Li et al. (2010) that those areas are possibly related to space weathering, or question the behavior of UV spectrum of weathered materials (Hendrix and Vilas, 2006). Of course, the space weathering spectral bluing in the UV was based on the comparisons between S-type asteroids and ordinary chondrites, and the compositional difference between Vesta and S-type asteroids might be another explanation.

5. Conclusions

We present a comprehensive view of new and existing observations of Vesta in the regime 0.2 − 1μm. The findings can be summarized as follows:

The geometric albedo derived from photometric and spectroscopic measurements by Swift/UVOT, HST, and IUE between 220 nm and 950 nm in wavelengths are consistent with each other, and consistent with previous measurements in the visible and in the UV.

The rotationally averaged geometric albedo of Vesta is 0.09 at 250 nm, 0.14 at 300 nm, 0.26 at 373 nm, 0.38 at 673 nm, and 0.30 at 950 nm. This is in line with UV albedos measured for other asteroids in the UV region, typically below 0.1. The UV spectrum of Vesta appears to have different characteristics from all other asteroids that were observed intensively in the UV recently, including Ceres, Steins, Lutetia, and Scheila.

Reanalysis of IUE spectra together with our rotational lightcurves in the visible does not show a reversal of the maximum and minimum of Vesta's lightcurve in the UV. Instead, the amplitude of Vesta's rotational lightcurve remains ~10% throughout UV-visible wavelengths, and decreases to ~6% near the 1-µm band center. The lightcurve maximum occurs in the eastern hemisphere and the minimum occurs in the western hemisphere. The linear spectral slope of Vesta between 240 nm and 320 nm displays a correlation with longitude, with the bluest area concentrated near 20° longitude, the reddest area in the eastern hemisphere, and moderately red area in the western hemisphere. This is entirely consistent with the distribution of spectral slope in the visible wavelengths from 439 nm to 673 nm, suggesting that the spectral slope map reported by Li et al. (2010) might remain similar into the UV.

Together with the nearly constant amplitude of Vesta's rotational lightcurve in the UV through visible wavelengths as well as the lack of reversal of lightcurve maximum and minimum, the correlation of spectral slope between UV and visible wavelengths does not support significant reversal of the spectral slope in the UV relative to the visible wavelengths on a global scale (Hendrix et al., 2003). If space weathering does cause spectral slope reversal from UV to visible, then the lack of such a phenomenon on Vesta suggests the lack of global-scale space weathering.

In the range of 200 to 1000 nm, our rotationally averaged spectrum of Vesta can be well explained by a single-component fine-grained howardite, or a linear mixing model with a small fraction of fine-grained diogenite added. This is consistent with previous conclusions about the global surface composition of Vesta (Gaffey, 1997).

Finally, we want to point out that the main conclusions of this research rely on the combination of UV and visible spectral regions. The diversity of the spectral properties of asteroids in the UV suggests that this spectral range could reveal substantial clues to the surface compositions and evolution of asteroidal surfaces. It is necessary to systematically collect observational data of asteroids in the UV and to expand our spectral library from laboratory UV measurements.

References

A'Hearn, M.F., and 11 colleagus, 2010. The far-ultraviolet albedo of Šteins measured with Rosetta-ALICE. Planet. Space Sci. 58, 1088-1096.

Binzel, R.P., Gaffey, M.J., Thomas, P.C., Zellner, B.H., Storrs, A.D., Wells, E.N., 1997. Geological mapping of Vesta from 1994 Hubble Space Telescope images. Icarus 128, 95-103.

Blanco, C., Catalano, S., 1979. UBV photometry of Vesta. Icarus 40, 359-363.

Bodewits, D., Kelley, M.S., Li, J.-Y., Landsman, W.B., Besse, S., A'Hearn, M.F., 2011a. Collisional excavation of asteroid (596) Scheila. Astrophys J. 733, L3.

Bodewits, D., Villanueva, G.L., Mumma, M.J., Landsman, W.B., Carter, J.A., Read, A.M., 2011b. Swift-UVOT grism spectroscopy of comets: A first application to C/2007 N3 (Lulin). Astron. J. 141, 12.

Bowell, E., Hapke, B., Domingue, D., Lumme, K., Peltoniemi, J., Harris, A.W., 1989. Application of photometric models to asteroids. In: Binzel, R.P., Gehrels, T., Matthews, M.S., (Eds.). Asteroids II. Univ. of Arizona Press, Tucson, pp. 524-556.

Breeveld, A.A., Landsman, W., Holland, S.T., Roming, P., Kuin, N.P.M., Page, M.J., 2011. An updated ultraviolet calibration for the Swift/UVOT. arXiv: 1102.4717v1 [astro-ph.IM]

Bus, S.J., Binzel, R.P., 2002. Phase II of the Small Main-Belt Asteroid Spectroscopic Survey, a feature-based taxonomy. Icarus 158, 146-177.

Bus, S., Binzel, R.P., 2003. Small Main-Belt Asteroid Spectroscopic Survey, Phase II. EAR-A-I0028-40SBN0001/SMASSII-V1.0. NASA Planetary Data System, 2003.

Butterworth, P.S., Meadows, A.J., Hunt, G.E., Moore, V., Willis, D.M., 1980. Ultraviolet spectra of asteroids. Nature 287, 701-703.

Butterworth, P.S., Meadows, A.J., 1985. Ultraviolet reflectance properties of asteroids. Icarus 62, 305-318.

Chapman, C.R., 1996. S-type asteroids, ordinary chondrites, and space weathering: The evidence from *Galileo*'s fly-bys of Gaspra and Ida. Meteorit. Planet. Sci. 31, 699-725.

Chapman, C.R., 2004. Space weathering of asteroid surfaces. Annu. Rev. Earth Planet.Sci. 32, 539–567.

Clark, B.E., and 11 colleagues, 2001. Space weathering on Eros: Constraints from albedo and spectral measurements of Psyche crater. Meteorit. Planet. Sci. 36, 1617-1637.

Cloutis, E.A., McCormack, K.A., Bell, J.F., III., Hendrix, A.R., Bailey, D.T., Craig, M.A., Mertzman, S.A., Robinson, M.S., Riner, M.A., 2008. Ultraviolet spectral reflectance properties of common planetary minerals. Icarus 197, 321-347.

Dressel, L., 2010. Wide Field Camera 3 Instrument Handbook, Version 3.0 (Baltimore: STScI).

Drummond, J.D., Fugate, R.Q., Christou, J.C., 1998. Full adaptive optics images of asteroids Ceres and Vesta: Rotational poles and triaxial ellipsoid dimensions. Icarus 132, 80-99.

Drummond, J.D., Christou, J., 2008. Triaxial ellipsoid dimensions and rotational poles of seven asteroids from Lick Observatory adaptive optics images, and of Ceres. Icarus 197, 480-496.

Festou, M.C., Stern, S.A., Tozzi, G.P., 1991. Asteroid 4 Vesta: Simultaneous visible and ultraviolet IUE observations. Icarus 94, 218-231.

Gaffey, M.J., 1997. Surface lithologic heterogeneity of Asteroid 4 Vesta. Icarus 127, 130-157.

Helfenstein, P., Veverka, J., 1989. Physical characterization of asteroid surfaces from photometric analysis. In: Binzel, R.P., Gehrels, T., Matthews, M.S., (Eds.). Asteroids II. Univ. of Arizona Press, Tucson, pp. 557-593.

Hendrix, A.R., Vilas, F., Festou, M.C., 2003. Vesta's UV lightcurve: hemispheric variation in brightness and spectral reversal. Icarus 162, 1-9.

Hendrix, A.R, Vilas, F., 2006. The effects of space weathering at UV wavelengths: S-class asteroids. Astrophys. J. 132, 13961404.

Hiroi, T., Pieters, C.M., Takeda, H., 1994. Grain size of the surface regolith of Asteroid 4 Vesta estimated from its reflectance spectrum in comparison with HED meteorites. Meteoritics 29, 394-396.

Keil, K., 2002. Geological history of Asteroid 4 Vesta: The "smallest terrestrial planet". In: Bottke, W.F., Jr., Cellino, A., Paolicchi, P., Binzel, R.P. (Eds.), Asteroids III. Univ. of Arizona Press, Tucson, pp. 573-584.

Keller, H.U., and 46 colleagues, 2010. E-type asteroid (2867) Steins as imaged by OSIRIS on board Rosetta. Science 327, 190-193.

Krist, J., Hook, R., 2004. TinyTIM users guide.

Lagerkvist, C.-I., Magnusson, P., Belskaya, I., Erikson, A., Dahlgren, M., Barucci, M.A., Asteroid photometric catalog (3rd update). EAR-A-3-DDR-APC-LIGHTCURVE-V1.0. NASA Planetary Data System, 1995.

Lean, J., 1989. Contribution of ultraviolet irradiance variations to changes in the Sun's total irradiance. Science 244, 197-200.

Li, J.-Y., McFadden, L.A., Parker, J.Wm., Young, E.F., Stern, S.A., Thomas, P.C., Russell, C.T., Sykes, M.V., 2006. Photometric analysis of 1 Ceres and surface mapping from HST observations. Icarus 182, 143-160.

Li, J.-Y., McFadden, L.A., A'Hearn, M.F., Feaga, L.M., Russell, C.T., Coradini, A., De Sanctis, C., Ammannito, E., 2009. UV absorption features of asteroid 1 Ceres, in 40th Lunar and Planetary Science Conference, The Woodlands, TX, abstract 2101.

Li, J.-Y., McFadden, L.A., Thomas, P.C., Mutchler, M.J., Parker, J.Wm., Young, E.F., Russell, C.T., Sykes, M.V., Schmidt, B.E., 2010. Photometric mapping of Asteroid (4) Vesta's southern hemisphere with Hubble Space Telescope. Icarus 208, 238-251.

Li, J.-Y., Thomas, P.C., Carcich, B., Mutchler, M.J., McFadden, L.A., Russell, C.T., Weinstein-Weiss, S.S., Rayman, M.D., Raymond, C.A., 2011. Improved measurement of asteroid (4) Vesta's rotational axis orientation. Icarus 211, 528-534.

Massa, D., Fitzpatrick, E.L., 2000. A recalibration of *IUE* NEWSIPS low-dispersion data. Astrophys. J. 126, 517-535.

McCord, T.B., Adams, J.B., Johnson, T.V., 1970. Asteroid Vesta: Spectral reflectivity and compositional implications. Science 178, 745-747.

Nesvorný, D., Jedicke, R., Whiteley, R.J., Ivezić, Ž., 2005. Evidence for asteroid space weathering from the Sloan Digital Sky Survey. Icarus 173, 132-152.

Nichols, J.S., Linsky, J.L., 1996. The final archive and recalibration of the International Ultraviolet Explorer (IUE) satellite. Astron. J. 111, 517-536.

Parker, J.W., Stern, S.A., Thomas, P.C., Festou, M.C., Merline, W.J., Young, E.F., Binzel, R.P., Lebofsky, L.A., 2002. Analysis of the first disk-resolved images of Ceres from ultraviolet observations with the Hubble space telescope. Astron. J. 123, 549-557.

Pieters, C.M., Taylor, L.A., Noble, S.K., Keller, L.P., Hapke, B., Morris, R.V., Allen, C.C., McKay, D.S., Wentworth, S., 2000. Space weathering on airless bodies: Resolving a mystery with lunar samples. Meteorit. Planet. Sci. 35, 1101-1107.

Pieters, C.M., Binzel, R.P., Bogard, D., Hiroi, T., Mittlefehldt, D.W., Nyquist, L., Rivkin, A., Takeda, H., 2005. Asteroid-meteorite links: the Vesta conundrum(s). Proc. IAU Symp. 229, 273-268.

Poole, T.S., and 30 colleagues, 2008. Photometric calibration of the Swift ultraviolet/optical telescope. Mon. Not. R. Astron. Soc. 383,627-645.

Rajan, A., et al., 2010. WFC3 data handbook. Version 2.0, (Baltimore: STScI).

Reddy, V., and 11 colleagues, 2011. Photometric, spectral phase and temperature effects on Vesta and HED meteorites: Implications for Dawn Mission. In preparation.

Rivkin, A.S., Li, J.-Y., Milliken, R.E., Lim, L.F., Lovell, A.J., Schmidt, B.E., McFadden, L.A., Cohen, B.A., 2011. The surface composition of Ceres. Space Sci. Rev., in press.

Roettger, E.E., Buratti, B.J., 1994. Ultraviolet spectra and geometric albedos of 45 asteroids. Icarus 112, 496-512.

Russell, C.T., and 15 colleagues, 2007. Dawn mission to Vesta and Ceres. Earth Moon Planets 101, 65-91.

Schevchenko, V.G., Tedesco, E.F., 2006. Asteroid albedos deduced from stellar occultations. Icarus 184, 211-220.

Stern, S.A., and 13 colleagues, 2011. Ultraviolet discoveries at asteroid (21) Lutetia by the Rosetta Alice UV spectrograph. Astron. J., in press.

Tedesco, E.F., Noah, P.V., Noah, M., Price, S.D., 2002. The supplemental *IRAS* minor planet survey. Astron J. 123, 1056-1085.

Thomas, P.C., Binzel, R.P., Gaffey, M.J., Storrs, A.D., Wells, E.N., Zellner, B.H., 1997. Vesta: Spin pole, size, and shape from HST images. Icarus 128, 88-94.

Vernazza, P., Brunetto, R., Strazzulla, G., Fulchignoni, M., Rochette, P., Meyer-Vernet, N., Zouganelis, I., 2006. Asteroid colors: a novel tool for magnetic field detection? The case of Vesta. Astron. Astrophys. 451, L43-L46.

Wagner, J.K., Hapke, B.W., Wells, E.N., 1987. Atlas of reflectance spectra of terrestrial, lunar, and meteoritic powders and frosts from 92 to 1800 nm. Icarus 69, 14-28.

Weaver, H.A., and 12 colleagues, 2010. Ultraviolet and visible photometry of asteroid (21) Lutetia using the Hubble Space Telescope. Astron. Astrophys. 518, A4.

Table 1. List of HST/WFC3 and Swift/UVOT observations

Date	Filter	Exposure Time (s)	Heliocentric Distance (AU)	Earth Range (AU)	Phase Angle (°)	Sub-Earth Latitude (°)	Sub-Solar Latitude (°)	Energy enclosure at 0.8" (radius)	$F_{\oplus}$ (W/m²/nm)	Equivalent wavelength (nm)	1-σ Bandwidth (nm)
HST WFC3 Observations											
Feb 25, 2010	F225W	45	2.39	1.42	5.3	23	27	92.5%	0.07240	252.5	-22.7, +19.8
Feb 25, 2010	F275W	10						92.3%	0.2357	282.3	-19.5, +14.1
Feb 25, 2010	F336W	1.7						92.8%	0.8720	337.7	-16.9, +17.1
Feb 25/28, 2010	F373N	12			5.3,			93.1%	1.032	373.0	±0.9
Feb 25/28, 2010	F469N	4			6.4			93.7%	1.970	468.8	±1.0
Feb 25/28, 2010	F673N	1.2						94.4%	1.505	676.6	±2.1
Feb 25/28, 2010	F953N	12						94.1%	0.8226	953.5	±3.6
Swift Observations											
Apr 5/20, 2011	UVM2	~128	2.16, 2.17	2.22, 2.05	26.4, 27.4	-30, -31	-20, -22	N/A	0.04622	244.9	-20.9, +30.1
	UVW2	13 – 68							0.08364	283.9	-61.9, +35.1
	Grism	~700							N/A	N/A	N/A

Figure captions

Fig 1 - Swift grism spectra of Vesta at three sub-Earth longitudes, compared with a rotationally
averaged IUE spectrum. The error bars are point-to-point uncertainties due to photon noise.
The spike at ~215 nm in the spectrum of 68° longitude is due to a background star and should
be ignored. The down-turn in all Swift spectra longward of ~290 nm is due to coincident
loss caused by the brightness of Vesta. Overall, Swift spectra are similar in shape to the IUE
spectrum in the overlapping wavelengths. Swift systematically measured lower geometric
albedos than IUE. This is most likely related to the systematic uncertainty of the two
instruments, and is within the photometric calibration uncertainty of 25%.

Fig 2 - Panel (a) shows the UV-visible geometric albedo spectrum of Vesta from HST/WFC3,
Swift/UVOT wideband photometry and grism spectroscopy, IUE, and SMASS II. Panel (b)
amplifies the UV region. The SMASS II spectrum is scaled to match HST measurement at
469 nm and 673 nm. All other geometric albedo measurements are photometrically
calibrated and not scaled. The y-error bars of photometric data points represent the
photometric calibration uncertainties. The y-error bars of HST points in 253 nm, 282 nm,
and 338 nm also include the estimated lightcurve amplitude of ~10%, with our data points
near the minima. The x-error bars of photometric points represent the 1-σ bandwidths as
described in the text. The y-error bars of spectra represent the relative uncertainties caused
by photon noise. The absolute photometric uncertainties of the Swift spectrum is ~25%, and
the IUE spectrum ~15-25%. Structures in the UV spectra from both Swift and IUE are
probably spectral features from the reference solar spectrum rather than real absorption
features in Vesta's spectrum.

Fig 3 - Panel (a) shows the rotational lightcurves of Vesta at various wavelengths from HST/WFC3 and Swift/UVOT broadband photometry, plotted with respect to sub-Earth (east-)longitude. The filters used are marked on the right-hand side of the plot. The three filled triangles mark the longitudes of the Swift grism spectra shown in Fig. 3. Panel (b) shows the rotational lightcurves of Vesta in three wavelength regions extracted from IUE spectra. The lightcurve amplitude of Vesta remains ~10% from UV to visible wavelengths.

Fig 4 - Panel (a) shows the comparison between the Vesta spectrum from 220 nm to 953 nm and the spectra of howardite and diogenite with various grain size. The small grain howardite fits the spectrum of Vesta the best. Panel (b) shows the various mixing models to fit the UV-visible spectrum of Vesta. The spectrum of linear mixing model with 80% small grain howardite and 20% small grain diogenite is similar to a single component small grain howardite, and fits Vesta's spectrum equally well. While the models with large grain components (Hendrix et al., 2003) fit the UV part well, they do not fit the 1-μm absorption or the spectral slope from 450 nm to 650 nm.

Fig 5 - UV spectral slope of Vesta between 240 nm and 320 nm measured from IUE spectra, plotted with respect to sub-Earth longitude. The slope is expressed as percentage per 100 nm at 280 nm. The dip near 20°, the relatively high slope in the eastern hemisphere and moderately high slope in the western hemisphere all appear to be real and correspond the spectrally blue, red, and moderately red spectral slopes in the visible wavelengths in similar longitudes.
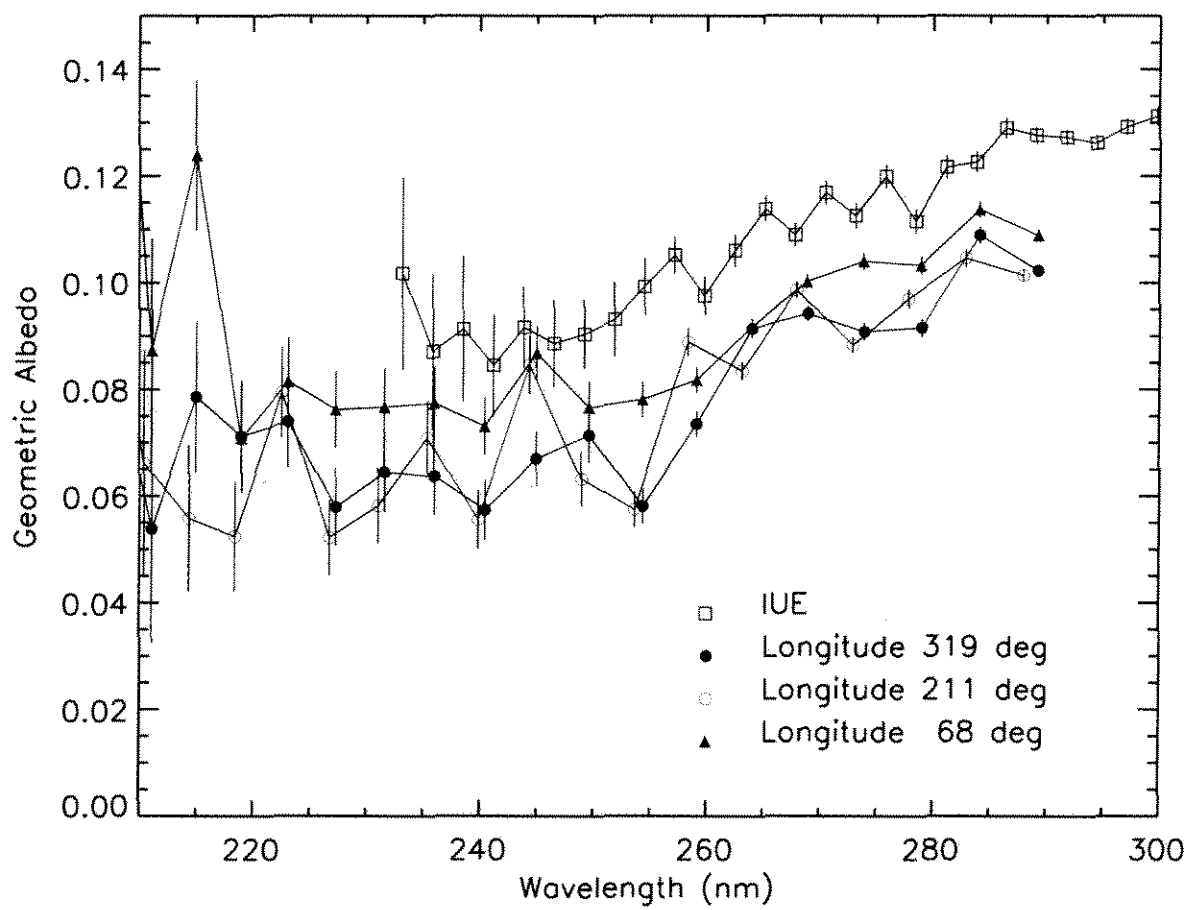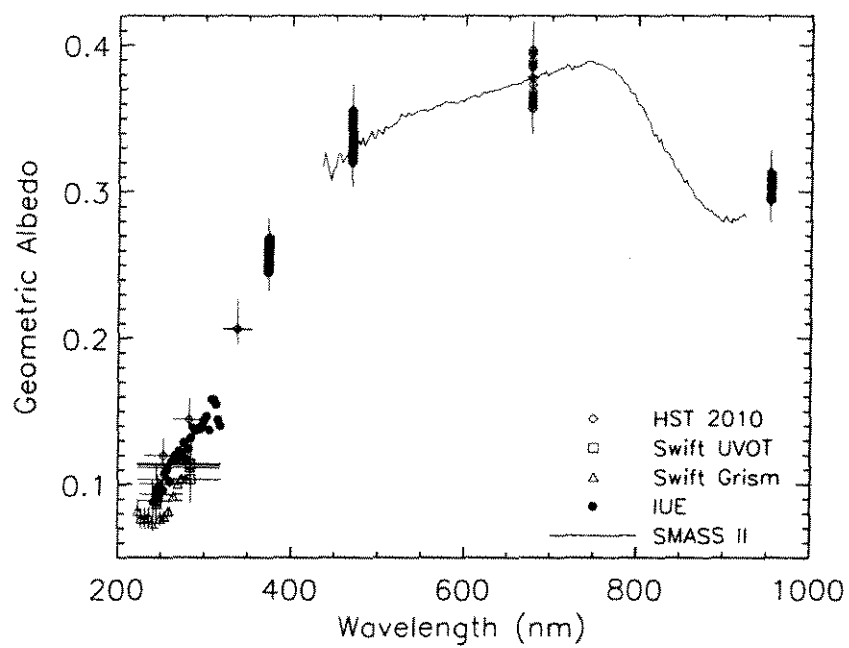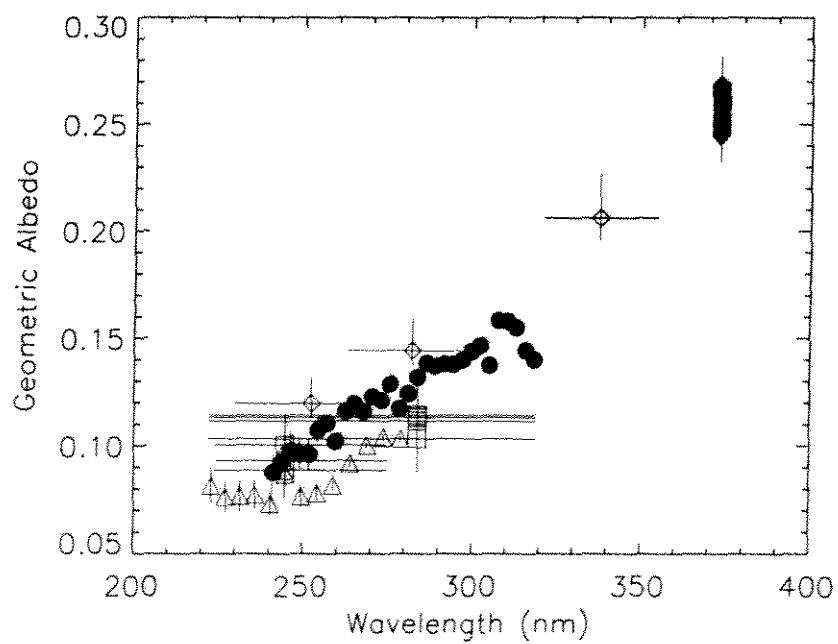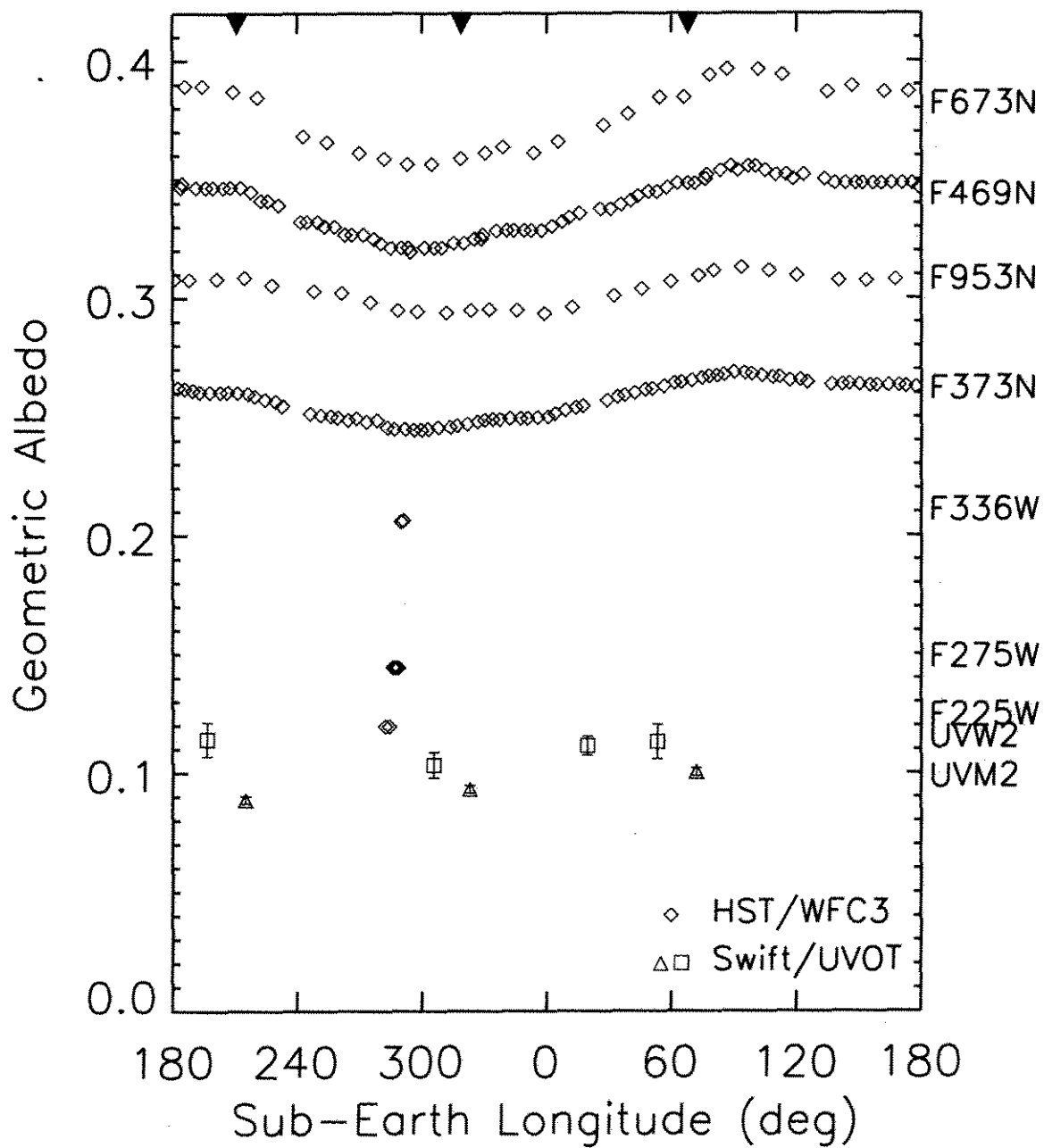
Fig. 1

Fig. 2

(a)

(b)

Fig. 3a

Fig. 4

(a)

(b)

Fig. 5

UV slope (%/100 nm at 280 nm)